Brazilian Journal
of Chemical
Engineering

ISSN 0104-6632
Printed in Brazil
www.abeq.org.br/bjche

Vol. 31, No. 03, pp. 757 - 769, July - September, 2014
dx.doi.org/10.1590/0104-6632.20140313s00002802

CATALYTIC OXIDATION OF VOLATILE ORGANIC COMPOUNDS (n-HEXANE, BENZENE, TOLUENE, o-XYLENE) PROMOTED BY COBALT CATALYSTS SUPPORTED ON γ-Al_2O_3-CeO_2

R. Balzer[1*], L. F. D. Probst[1], V. Drago[2], W. H. Schreiner[3] and H. V. Fajardo[4]

[1]Department of Chemistry, Universidade Federal de Santa Catarina, 88040-900, Florianópolis - SC, Brasil.
Phone: + (55) (48) 3721-9966, Fax: + (55) (48) 3721-6850
E-mail: rosanabalzer@gmail.com
[2]Department of Physics, Universidade Federal de Santa Catarina, 88040-900, Florianópolis - SC, Brasil.
[3]Department of Physics, Universidade Federal do Paraná, 81531-970, Curitiba - PR, Brasil.
[4]Department of Chemistry, Universidade Federal de Ouro Preto, 35400-000, Ouro Preto - MG, Brasil.

(Submitted: June 26, 2013 ; Revised: October 10, 2013 ; Accepted: November 18, 2013)

Abstract - Cobalt catalysts supported on γ-alumina, ceria and γ-alumina-ceria, with 10 or 20%wt of cobalt load, prepared by the wet impregnation method and characterized by X-ray diffraction (XRD), scanning electron microscopy (SEM), field emission transmission electron microscopy (FETEM), N_2 adsorption-desorption isotherms (BET/BJH methods), energy-dispersive X-ray spectroscopy (EDX), X-ray photoemission spectroscopy (XPS), O_2-chemisorption and temperature programmed reduction (TPR) were used to promote the oxidation of volatile organic compounds (n-hexane, benzene, toluene and o-xylene). For a range of low temperatures (50-350 °C), the activity of the catalysts with a higher cobalt load (20% wt) was greater than that of the catalysts with a lower cobalt load (10% wt). The Co/γ-Al_2O_3-CeO_2 catalytic systems presented the best performances. The results obtained in the characterization suggest that the higher catalytic activity of the Co_{20}/γ-Al_2O_3-CeO_2 catalyst may be attributed to the higher metal content and amount of oxygen vacancies, as well as the effects of the interaction between the cobalt and the alumina and cerium oxides.
Keywords: Heterogeneous catalysis; Oxidation; Volatile organic compounds; Cobalt catalysts.

INTRODUCTION

Volatile organic compounds (VOCs) are dangerous and highly toxic pollutants generated during a variety of industrial and agricultural activities as well as energy use, including that associated with transportation, among other practices (Kim, 2002; Garcia-Vazquez *et al*., 2004; Kim and Shim, 2010; Liotta, 2010). Therefore, there is a need for the development of techniques which are both economically feasible and able to effectively destroy these pollutants rather than simply remove them. Catalytic oxidation has been acknowledged as the most effective method to reduce VOC emissions. The desired reaction products are carbon dioxide (CO_2) and water (H_2O) since they are not harmful to the environment (Calvo *et al*., 2004; Garcia-Vazquez *et al*., 2004; Kim and Shim, 2010).

Catalysts such as platinum (Pt) and palladium (Pd) are typically used to promote these reactions. However, due to the high cost of these metals, they are increasingly being replaced with cheaper catalysts employing transition metals, such as manganese (Mn), nickel (Ni), chromium (Cr) and cobalt (Co). These metals, which have a high oxidation potential, can be supported in matrices with a high surface area, notably alumina (Al_2O_3) and silica (SiO_2) (Kim,

*To whom correspondence should be addressed
Postal Address: Universidade Federal de Santa Catarina, UFSC, Centro de Ciências Físicas e Matemáticas, CFM, Departamento de Química, Campus Universitário Trindade, 88040-900, Florianópolis, SC - Brazil.

2002; Calvo *et al*., 2004; Garcia-Vazquez *et al*., 2004; Kim and Shim, 2010). Therefore, the development of new catalysts that provide these conditions and exhibit superior performance in industrial processes is an important challenge confronting researchers.

It has been reported in the literature that CeO_2 has the potential to increase the degree of oxidation in reactions, due to the creation of active oxygen (Setiabudi *et al*., 2004). The catalytic activity of CeO_2 has also been attributed to its ability to store and release oxygen. Therefore, the incorporation of CeO_2 can improve the performance of the redox catalyst, besides acting as a stabilizer of O_2 on the surface of the material (Kirchnerova *et al*., 2002; Kirchnerova and Klvana, 2000).

In this context, in order to contribute to the development of heterogeneous catalysts to promote the oxidation of VOCs, in this study the potential of cobalt-based catalysts supported on γ-Al_2O_3, CeO_2 and especially γ-Al_2O_3-CeO_2 for the conversion of n-hexane, benzene, toluene and o-xylene to CO_2 and H_2O was investigated. These organic compounds were chosen as model compounds to be used in this study due to their action as greenhouse gases and their toxic, carcinogenic and molecular characteristics (Wu *et al.*, 2011; Genuino *et al.,* 2012). The effect of the cobalt content on the textural properties of the catalysts and on the catalytic performance was also investigated.

EXPERIMENTAL

Catalyst Preparation

The cobalt catalysts were prepared via the wetness impregnation technique with different amounts of cobalt, that is, 10% and 20%. The γ-Al_2O_3-CeO_2 support used was obtained by blending (by mechanical mixing) two oxides: γ-alumina (Engelhard Exceptional Technologies®) with surface area (S_{BET}) = 208 m^2g^{-1}, pore volume (V_p) = 0.69 cm^3g^{-1} and pore diameter (D_p) = 6.63 nm; and cerium oxide (Riedel-de Haen®) with surface area (S_{BET}) = 4 m^2g^{-1}, pore volume (V_p) = 0.01 cm^3g^{-1} and pore diameter (D_p) = 6.38 nm. The γ-Al_2O_3:CeO_2 ratio (wt%) of the oxides was 1:1. The precursor salt, cobalt nitrate ($Co(NO_3)_2.6H_2O$ – Vetec®), was dissolved in distilled water and added to the support in appropriate amounts. The materials obtained were then dried for 24 hours at 100 °C, ground and sieved (between 177 and 210 μm). The samples obtained were calcined in a muffle furnace, without air circulation, starting at ambient temperature with a heating rate of 5 °C.min^{-1} up to 550 °C, maintaining this temperature for 4 hours.

Characterization of Catalysts

The crystalline structure of the catalysts was analyzed by X-ray powder diffraction (Bruker-AXS Siemens®) with CuKα radiation (V= 40kV; I=30mA). The morphology and microstructure of the catalysts were observed by scanning electron microscopy (SEM, JEOL JSM-6390LV) and field emission transmission electron microscopy (FETEM, JEOL JEM-1011). The specific surface area was determined by the BET method based on N_2 adsorption-desorption measurements taken at 77 K (Nova 2200e – Quantachrome Instruments®). The chemical composition and metal content of the catalysts were analyzed by energy-dispersive X-ray spectroscopy (EDX). The binding energy of the elements was studied by X-ray photoemission spectroscopy (XPS) (VG Microtech 3000). The temperature profile of the catalytic reduction was obtained on a ChemBET – TPR/TPD analyzer (Quantachrome Instruments®). The O_2-chemisorption was conducted at 600 °C using a ChemBET analyzer (Quantachrome Instruments®).

Catalyst Activity Test

The catalytic activity of the samples prepared in relation to the oxidation of VOCs (n-hexane, benzene, toluene and o-xylene) was measured in a fixed tubular quartz reactor (39.5 cm in length and 9 mm in inner diameter) under atmospheric pressure (Figure 1). The following conditions were chosen: catalyst 0.1 g, inlet n-hexane (Vetec®) concentration 2.0 g m^{-3}, benzene (Vetec®) concentration 2.5 g m^{-3}, toluene (Vetec®) concentration 0.65 g m^{-3} and o-xylene (Vetec®) concentration 0.45 g m^{-3} in air, gas flow rate of 20 cm^3 min^{-1} and 0.3s of residence time, gas hourly space velocity 12000 h^{-1}, and temperature range 50-350 °C. The reaction data were collected after at least 2 h on stream at room temperature. The products (CO_2 and H_2O) were analyzed by GC–MS and the reactants and product mixtures were analyzed on gas chromatographs equipped with an FID and TCD detector and an HP-5 column. The catalytic activity was expressed as the degree of hydrocarbon conversion, calculated as follows:

$$Hydrocarbons\,(\%) = \frac{[Hydrocarbons]_{in} - [Hydrocarbons]_{out}}{[Hydrocarbons]_{in}} \times 100\% \quad (1)$$

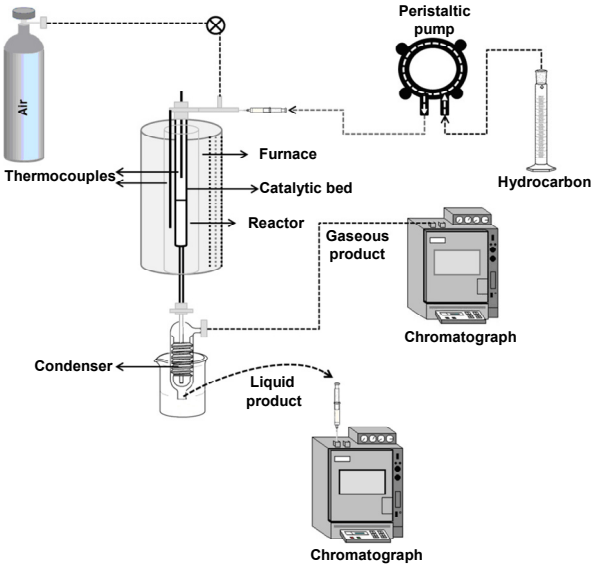

Figure 1: Schematic representation of the reaction unit used for the oxidation of VOCs.

RESULTS AND DISCUSSION

Characterization of the Catalysts

The X-ray diffraction patterns of the samples are shown in Figure 2. It can be observed that the peaks for the catalysts supported on alumina have low intensity and are broad, indicating that the material has a low crystallinity. The diffraction peaks at 2θ = 28, 33, 47, 56, 59, 69 and 88º are assigned to reflections related to the CeO_2 phase, a cubic crystal system (JCPDS data file 00-034-0394). These peaks have a higher definition and intensity, characteristic of a crystalline material. The peaks (2θ = 39 and 45°) are assigned to the reflections for the aluminum oxide phase, a cubic crystal system (JCPDS data file 01-074-2206). The peaks at 2θ = 31, 37, 59, 66 and 79º are characteristic of Co_3O_4 (JCPDS data file 01-075-0076). The peaks at 2θ = 31 and 59º suggest the presence of CoO with a cubic spinel-type structure. The intensity of the peak at 2θ = 33 for Co_3O_4 is higher for the Co_{20}/γ-Al_2O_3-CeO_2 sample compared with the Co_{10}/γ-Al_2O_3-CeO_2 sample. This suggests that the cobalt oxide on the Co_{20}/γ-Al_2O_3-CeO_2 surface has a higher crystallinity and larger particle size and also that the Co_3O_4 is well dispersed on the Co_{10}/γ-Al_2O_3-CeO_2 surface (Soykal *et al*., 2012a; Wang *et al*., 2007).

According to the calculations shown in Table 1, the size of the crystallite CoO and Co_3O_4 increases with the cobalt content in the case of cobalt supported on γ-Al_2O_3-CeO_2, ranging from 42 to 52 nm and 25 to 28 nm, respectively.

The TPR profiles for the samples, shown in Figure 3, show peaks at reduction temperatures higher than 300 °C. The steps involved in the reduction of Co_3O_4 are still controversial. There are two types of TPR spectrum for Co_3O_4 reported in the literature: a spectrum with one broad peak representing Co_3O_4 reduction in a single step and a spectrum with two peaks ascribed to a two-step reduction process ($Co_3O_4 \rightarrow CoO \rightarrow Co$) (Kang *et al*., 2003; Luo *et al*., 2008). The TPR for CeO_2 may contain one to three peaks. It is generally accepted that CeO_2 reduction at the surface occurs via a stepwise mechanism: firstly, the reduction of the outermost layer of Ce^{4+} produced at lower temperatures (peak at between 400-550 °C); secondly, the formation of non-stoichiometric oxides (Ce_yO_x) (peak at approximately 580-650 °C); and thirdly, the reduction of the inner Ce^{4+} (CeO_2 to Ce_2O_3 bulk reduction) associated with a peak at above 750 °C (Kang *et al*., 2003; Lovon *et al*., 2012; Luo *et al*., 2008).

However, according to Holgado *et al*. (2000), the latter TPR peak (highest temperature) could also be attributed to the reduction of CeO_2 to CeO_{2-x}.

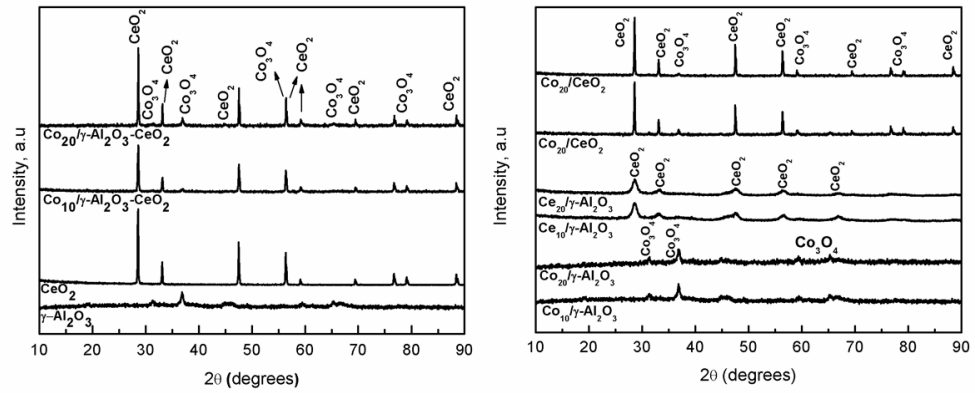

Figure 2: XRD patterns for the catalysts and supports.

Table 1: Textural data for the supported cobalt catalysts.

Sample	BET ($m^2 g^{-1}$)	Vp ($cm^3 g^{-1}$)	Dp (nm)	CoO average size (nm)[a]	Co_3O_4 average size (nm)[a]	CeO_2 average size (nm)[a]	Co average size (nm)[b]	Co loading (wt%)[c]	Co dispersion (%)[d]
Al_2O_3	208	0.69	6.63	-	-	-	-	-	-
CeO_2	4	0.01	6.38	-	-	-	-	-	-
Co_{10}/γ-Al_2O_3	184	0.63	6.07	-	-	-	-	-	-
Co_{20}/γ-Al_2O_3	130	0.42	6.47	-	-	-	-	-	-
Co_{10}/CeO_2	7	0.05	13.26	-	-	-	-	-	-
Co_{20}/CeO_2	7	0.03	10.24	-	-	-	-	-	-
Ce_{10}/γ-Al_2O_3	153	0.51	6.60	-	-	-	-	-	-
Ce_{20}/γ-Al_2O_3	142	0.43	6.08	-	-	-	-	-	-
Co_{10}/γ-Al_2O_3-CeO_2	74	0.24	6.45	42	25	50	96.63	9.6	0.99
Co_{20}/γ-Al_2O_3-CeO_2	65	0.19	6.00	52	28	>100	104.67	20	0.92

Vp = pore volume; Dp = pore diameter. [a] Calculated using XRD. [b] Calculated using HRTEM. [c] Calculated from semi-quantitative EDX data. [d] Calculated through a formula: ($D_{Co} = 6n_s.M_{Co}/\rho_{Co}.N_A.d_{Co}$) , where n_s is the number of Co atoms at the surface per unit area ($14.6x10^{18}$ at.m^{-2}); M_{Co} is the molar mass of cobalt (58.93 $gmol^{-1}$); ρ_{Co} is the density of cobalt (8.9 gcm^{-3}); N_A is Avogadro's number ($6.023x10^{23}$ mol^{-1}) and d_{Co} is the average Co size (determined by HRTEM).

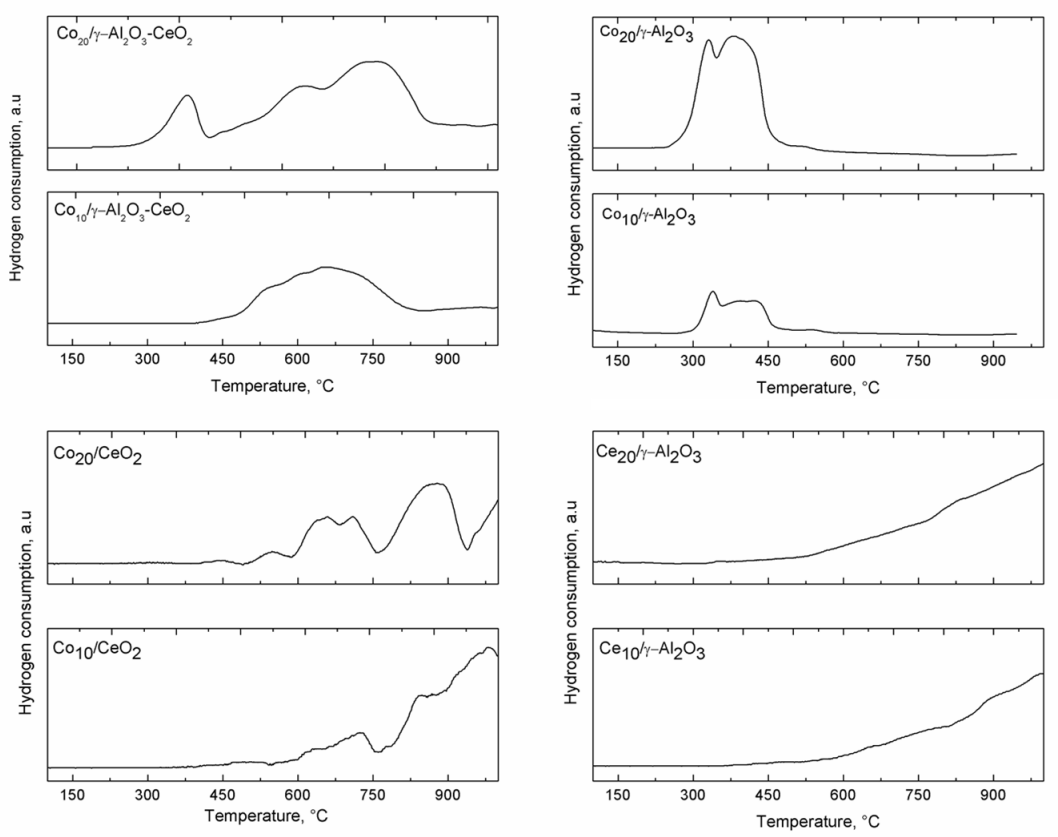

Figure 3: TPR profiles for the catalysts.

The TPR profiles of the Co_{10}/γ-Al_2O_3 and Co_{20}/γ-Al_2O_3 samples display two main reduction peaks. The first one, with a maximum at around 340 °C, corresponds to the reduction of the Co_3O_4 phase to CoO and a broad peak, centered at around 400 °C, corresponds to the reduction of CoO to Co^0. Reduction peaks at above 700 °C, corresponding to the reduction of a mixed phase of cobalt oxide-aluminum oxide (non-stoichiometric aluminate) (Hu and Lu, 2010; Garcia and Assaf, 2012), were not observed. The TPR profiles for the Co_{10}/CeO_2 and Co_{20}/CeO_2 samples show four major H_2 consumption peaks. The lower-temperature peak can be attributed to the reduction of the Co_3O_4 phase to CoO, as well as the

reduction of surface CeO_2, while the second peak is assigned to the subsequent reduction of CoO to Co^0. Finally, the third peak at around 595 °C indicates the reduction of Co^{2+} or Co^{3+} ions in a strong interaction with CeO_2, which could also inhibit the reduction of CeO_x species. The higher-temperature peak can be ascribed to the reduction of Ce^{4+} to Ce^{3+} in the bulk of the ceria (Spadaro *et al*., 2005; Lovon *et al*., 2012). The TPR profile for the Co_{10}/γ-Al_2O_3-CeO_2 sample shows a broad peak with three shoulders centered at 540, 600 and 670 °C. The first of these can be attributed to the reduction of Co_3O_4 to CoO and different interactions with the support, while the second indicates the reduction of Co^{2+} or Co^{3+} ions to metallic Co, as well as the reduction of non-stoichiometric species of cerium oxide. The TPR profile for the Co_{20}/γ-Al_2O_3-CeO_2 sample shows three major H_2 consumption peaks. The first peak at 375 °C can be attributed to the reduction of the independent Co_3O_4 phase that weakly interacts with CeO_2 directly to Co^0, which may be due to the high cobalt content of the sample. The second peak, centered at 590 °C, results from the reduction of Co^{2+} or Co^{3+} ions strongly bound to the ceria matrix to Co^0. However, this second peak could also represent the reduction of non-stoichiometric species, as mentioned above. For both samples, the TPR peak at the highest temperature can be ascribed to the reduction of bulk CeO_2 (Luo *et al*., 2008). The TPR peaks of the Ce_{10}/γ-Al_2O_3 and Ce_{10}/γ-Al_2O_3 samples have low intensity, presenting a flatter profile compared to those of the other samples. The broad peak observed at around 750-900 °C could be attributed to the reduction of bulk CeO_2. It is interesting to note that the TPR profiles for the Co_{10}/γ-Al_2O_3-CeO_2 and Co_{20}/γ-Al_2O_3-CeO_2 samples show that the reduction peaks shift to lower temperatures as the cobalt loading decreases. It has been found that the higher the dispersion and the smaller the size of the metal oxide particles, the lower the reduction peak temperature of the metal oxide in the TPR pattern will be (Kang *et al*., 2003; Soykal *et al*., 2012b). In addition, the shift to a lower reduction temperature observed for Co_{10}/γ-Al_2O_3-CeO_2 can also be ascribed to the higher surface ceria concentration as well as the smaller size of the crystallites present in this sample, as indicated by the XRD and XPS measurements, respectively (Tables 1 and 2) (Abbasi *et al.*, 2011). The position and intensity of the hydrogen consumption peaks may also indicate the surface oxygen mobility of some oxides, such as CeO_2. An increase in the surface oxygen mobility may lead to a decrease in the temperature at which the reduction peak appears, due to a decrease in the crystal size in the sample. Thus, in our case, the surface oxygen species of Co_{10}/γ-Al_2O_3-CeO_2 appear to be more active than those of Co_{20}/γ-Al_2O_3-CeO_2 (Mamontov *et al*., 2000; Sun *et al*., 2008). This is in agreement with the results presented in Table 1. On the other hand, the hydrogen consumption peaks located at higher temperatures may indicate a better contact (i.e., stronger interaction) between the cobalt and the cerium and aluminum oxides in the Co_{20}/γ-Al_2O_3-CeO_2 sample. The results for the TPR experiments indicate the possibility that different cobalt species are present and that the extent of the cobalt-support interaction is distinct for each species.

The values for the specific surface area, volume and average pore diameter of the catalysts are shown in Table 1. It can be seen that, in contrast to alumina, there was a decrease in the surface area, as well as in the volume and pore diameter, as the metal (cobalt) content in the samples increased and with addition of ceria to the alumina. This result may be related to the low surface area of ceria, and also the covering of the smaller pores of the alumina by the cerium and cobalt oxides. The reduction in the specific surface area of the samples with increasing cobalt content may also be associated with the replacement of Ce^{4+} ions by Co^{2+} and/or Co^{3+} ions, leading to an increase in the mole fraction of oxygen vacancies to maintain a neutral charge, which promotes an increase in the diffusion coefficient, resulting in an increase in the particle size (Marcos *et al*., 2004). The high surface area of the oxide support generally leads to an increased dispersion of the metal and this tendency was observed for the samples studied (Table 1). The isotherms for the Co_{10}/γ-Al_2O_3-CeO_2 and Co_{20}/γ-Al_2O_3-CeO_2 catalysts correspond to type IV (of the IUPAC classification), which is typical of mesoporous materials (Figure 4(a)). The appearance of a type H1 hysteresis loop was observed at high relative pressures ($P/P_o \approx 0.7$ to 0.9) and this can be attributed to the formation of textural mesoporosity. The pore size distribution curves (Figure 4(b)) for the catalysts exhibited a unimodal profile with a variation in the pore size, ranging from 2-50 nm, the pores being of regular cylindrical shape and/or polyhedral with open ends (Andreeva *et al*., 2001; Barreiro *et al*., 2004; Corma, 1997; Marcos *et al*., 2004).

The EDX analysis confirmed the presence of cobalt in the Co_{10}/γ-Al_2O_3-CeO_2 and Co_{20}/γ-Al_2O_3-CeO_2 catalysts and the theoretical values are in very good agreement with the experimental results, as shown in Table 1.

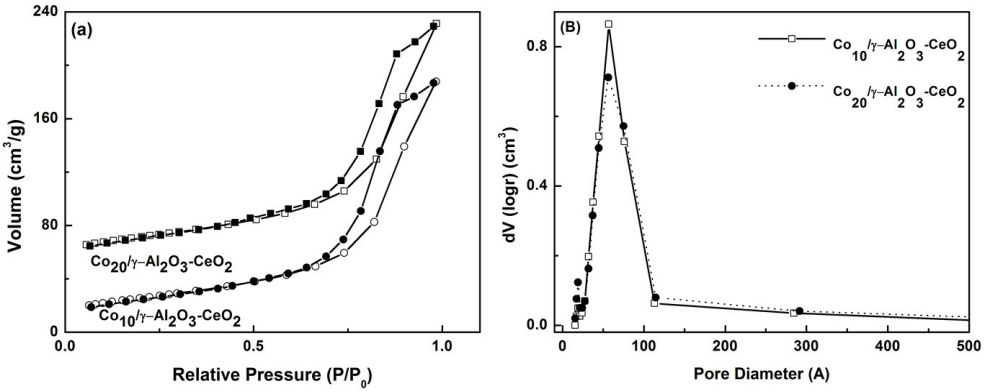

Figure 4: N_2 adsorption-desorption isotherms of the samples (a) and their pore size distribution curves obtained from the N_2 desorption isotherms using the BJH method (b).

The morphological properties of the catalysts were investigated by SEM and TEM. The SEM images obtained for the Co_{10}/γ-Al_2O_3-CeO_2 and Co_{20}/γ-Al_2O_3-CeO_2 samples (Figure 5) show irregular clusters both in form and size, featuring crumb-like particles with rugged surfaces.

Figure 6 shows the TEM images of the Co_{10}/γ-Al_2O_3-CeO_2 and Co_{20}/γ-Al_2O_3-CeO_2 samples. As shown in Figure 6(a), the catalysts obtained are polyhedral with irregular shapes. The most frequently observed fringes correspond to the (111), (311) and (220) crystallographic planes of CeO_2, CoO and Co_3O_4, respectively. The reflection attributed to the lattice plane (220) of CeO_2 can also be identified. The perimeter of contact between cobalt oxide and cerium oxide can be clearly identified in the images (Figs. 6 (b-d)). This indicates a strong interaction between the metal oxide and the support in the catalyst, and the formation of active sites can occur more easily during the reaction, which favors the catalytic activity. The histograms for the particle size distribution of cobalt in the catalysts are shown in Figs. 6 (e-f). The average particle sizes observed for Co_{10}/γ-Al_2O_3-CeO_2 and Co_{20}/γ-Al_2O_3-CeO_2 were 96.63 and 104.67 nm, respectively.

The chemical species present on the surfaces of the catalysts and some of their proportions were evaluated by XPS. Table 2 shows the binding energy values obtained for the Co_{10}/γ-Al_2O_3-CeO_2 and Co_{20}/γ-Al_2O_3-CeO_2 catalysts investigated. The detected levels of O1s, Al $2p_{1/2}$ 2p, $Ce3d_{5/2}$ and $Co2p_{3/2}$ showed a difference in the binding energies from one catalyst to another. The full-range XPS spectra of the catalysts are shown in Figure 7. The presence of the $Ce3d_{5/2}$ peak at 881.3eV for Co_{10}/γ-Al_2O_3-CeO_2 and at 887.6 and 904.0eV for Co_{20}/γ-Al_2O_3-CeO_2 characterize the presence of Ce^{+3} and Ce^{+4} in both catalysts (Beche *et al*., 2008; Beche *et al*., 2012). The $Co2p_{3/2}$ peak at 779.0eV for Co_{10}/γ-Al_2O_3-CeO_2 and 785.6eV for Co_{20}/γ-Al_2O_3-CeO_2 characterize the presence of Co^{2+} (Lakshmi *et al*., 2009; Salim and Khawaja, 1992). The peak at 535.8 and 536.3eV is characteristic of O_{1s}. The peaks at 74.5 and 74.6eV are characteristic of $Al2p_{1/2}$ 2p. The lower Al/O, Al-Ce/O and Co/O ratios observed for the Co_{10}/γ-Al_2O_3-CeO_2 catalyst may indicate greater oxygen enrichment at the surface, in relation to the interior of the sample compared with the Co_{20}/γ-Al_2O_3-CeO_2 catalyst.

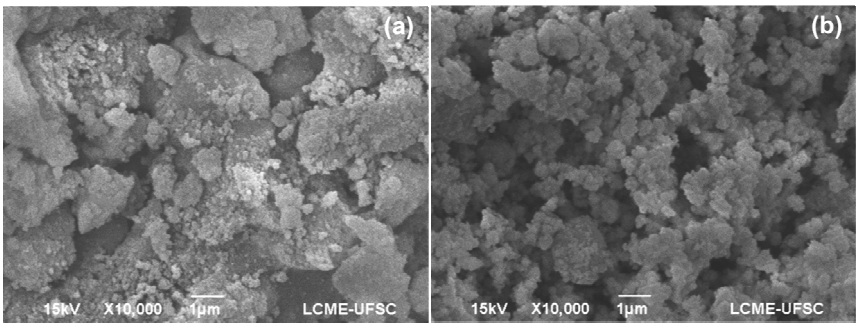

Figure 5: SEM images of Co_{10}/γ-Al_2O_3-CeO_2 (a) and Co_{20}/γ-Al_2O_3-CeO_2 (b).

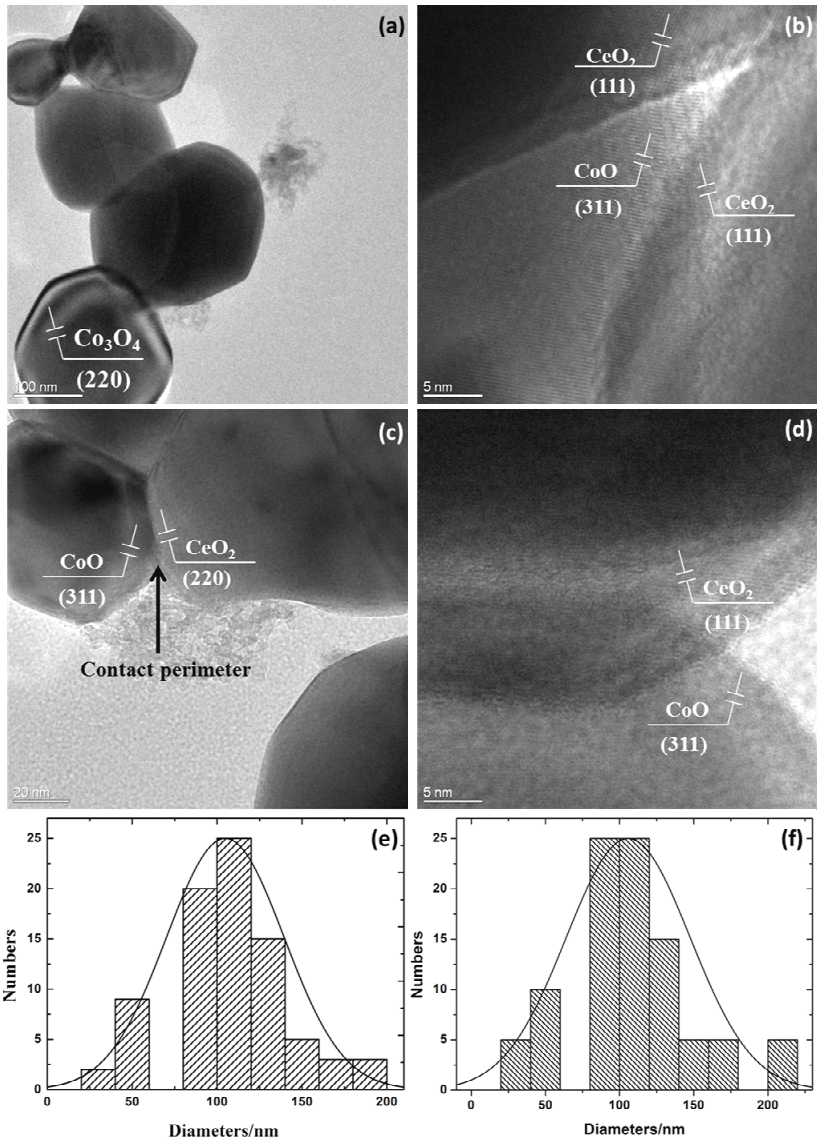

Figure 6: TEM images of Co_{10}/γ-Al_2O_3-CeO_2 (a-b) and Co_{20}/γ-Al_2O_3-CeO_2 (c-d). Particle size distribution of cobalt in Co_{10}/γ-Al_2O_3-CeO_2 (e) and Co_{20}/γ-Al_2O_3-CeO_2 (f).

Table 2: Binding energy values, surface composition and some relative atomic ratios for the solids studied, determined from XPS measurements.

Sample	Binding energy (eV)				Relative atomic ratios				
	O_{1s}	$Al2p_{1/2}$ 2p	$Ce3d_{5/2}$	$Co2p_{3/2}$	Co/Ce	Al/O	Ce/O	Al-Ce/O	Co/O
Co_{10}/γ-Al_2O_3-CeO_2	535.8	74.5	881.3	779.0	0.07	0.09	0.30	0.40	0.09
Co_{20}/γ-Al_2O_3-CeO_2	536.3	74.6	887.6/ 904.0	785.6	0.18	0.21	1.57	1.78	0.28
	Surface composition (at. %)								
	O		Al		Ce		Co		
Co_{10}/γ-Al_2O_3-CeO_2	61.09		29.99		7.56		1.35		
Co_{20}/γ-Al_2O_3-CeO_2	42.58		48.19		6.43		2.81		

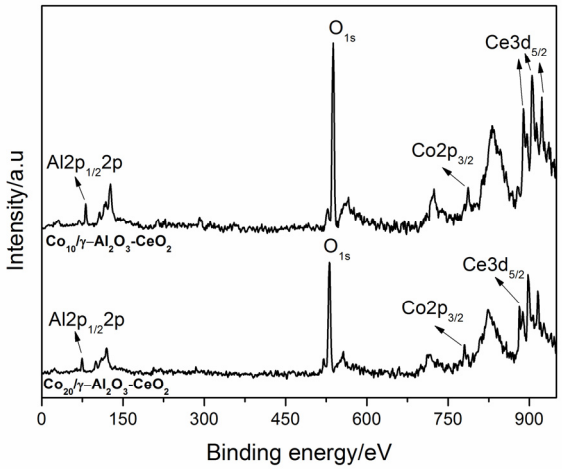

Figure 7: XPS spectra for the catalysts Co_{10}/γ-Al_2O_3-CeO_2 and Co_{20}/γ-Al_2O_3-CeO_2.

The surface composition of cobalt is 2.81% for Co_{20}/γ-Al_2O_3-CeO_2 and 1.35% for Co_{10}/γ-Al_2O_3-CeO_2, as expected due to the higher metal content of this catalyst. Table 2 also gives the Co/Ce ratio at the catalyst surfaces and the highest ratio can be observed for Co_{20}/γ-Al_2O_3-CeO_2, indicating cobalt enrichment at the surface in the case of this sample. On the other hand, a decrease in the Co/Ce ratio at the surface can be attributed to the partial coating of the cobalt oxide by cerium oxide (Todorova *et al*., 2010).

Table 3 reports the results obtained from oxygen chemisorption measurements. The oxygen storage capacity (OSC) was calculated based on oxygen uptake. These values allow us to estimate the total amount of oxygen available in the oxide catalyst (Zhang *et al.*, 2012). The Co_{20}/γ-Al_2O_3-CeO_2 catalyst has a larger OSC than the Co_{10}/γ-Al_2O_3-CeO_2 catalyst, indicating that the former has a higher amount of oxygen vacancies, as also observed from the N_2 physisorption results.

Catalytic Activity Tests

In order to investigate the catalytic activity of the samples synthesized, the oxidation of volatile organic compounds (n-hexane, benzene, toluene and o-xylene) was carried out. Figure 8 shows the VOC conversions for the catalysts as a function of the reaction temperature and Table 4 shows the light-off temperature (T_{50}) for oxidation of VOCs over the catalysts.

Table 3: Oxygen chemisorption measurements for the different catalysts.

Sample	Oxygen Storage Capacity ($mmol/m^2$)
Co_{10}/γ-Al_2O_3-CeO_2	1.30
Co_{20}/γ-Al_2O_3-CeO_2	3.24

Table 4: Temperatures for the 50% VOC conversion (T_{VOC50}) observed for the different catalysts.

Sample	$T_{n\text{-hexane}50}$(°C)	$T_{benzene50}$(°C)	$T_{toluene50}$(°C)	$T_{o\text{-xylene }30}$(°C)
Co_{10}/γ-Al_2O_3-CeO_2	125	200	200	250
Co_{20}/γ-Al_2O_3-CeO_2	105	175	200	225
Co_{10}/γ-Al_2O_3	325	350	> 350	> 350
Co_{20}/γ-Al_2O_3	290	320	> 350	335
Co_{10}/CeO_2	255	280	> 350	350
Co_{20}/CeO_2	220	230	> 350	310
Ce_{10}/γ-Al_2O_3	> 350	> 350	> 350	> 350
Ce_{20}/γ-Al_2O_3	> 350	> 350	> 350	> 350

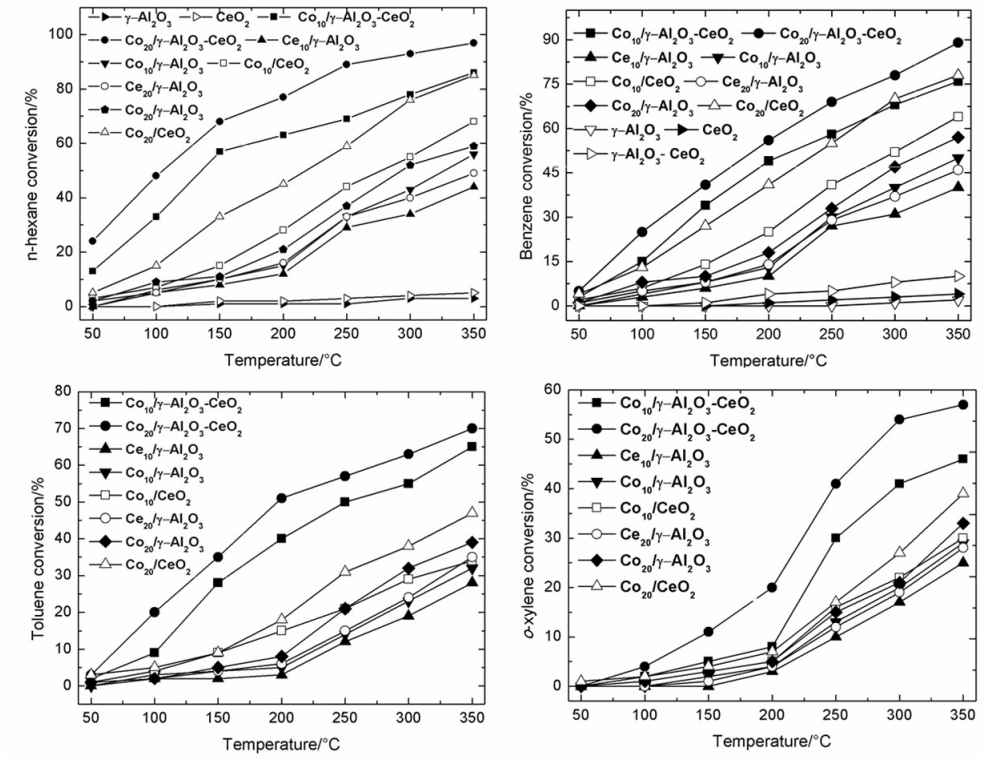

Figure 8: VOC conversion as a function of reaction temperature for different catalysts with the reaction performed under varying conditions: n-hexane 2.0 g m^3, benzene 2.5 g m^3, toluene 0.65 g m^3, o-xylene 0.45 g m^3. Total flow rate: 20 cm^3 min^{-1}.

It can be observed from the results given in Figure 8 that the catalysts were active in the VOC oxidation reactions and that a similar tendency was observed for all samples, that is, the VOC conversion increased with an increase in the reaction temperature, as expected. However, in all cases the best performance was observed for the catalysts supported on γ-Al_2O_3-CeO_2. Appropriate combinations of metal oxides as catalyst supports may provide higher activity in oxidation reactions than single oxides, as reported by several authors (Luo *et al*., 2008; Abbasi *et al*., 2011; Barakat *et al*., 2012). Therefore, the discussion on the catalytic tests was focused on the former type of catalyst. The catalyst with the highest cobalt load was the most active in all cases, regardless of the reaction temperature and the nature of the organic compound. It is clear from the data presented in Table 4 that the lowest light-off temperature was observed for the Co_{20}/γ-Al_2O_3-CeO_2 catalyst, even though this sample had the lowest specific surface area and cobalt dispersion. These findings can be attributed to the amount of cobalt species present in the catalysts and the interaction of Co_3O_4 and CoO with CeO_2, which varies according to the cobalt content, as observed from the XPS and TPR data. The surface properties of these catalysts are essential for analyzing the catalytic activity. The dispersion of cobalt in the catalyst ranged from 0.99% for Co_{10}/γ-Al_2O_3-CeO_2 to 0.92% for Co_{20}/γ-Al_2O_3-CeO_2. This shows that the metal dispersion decreased with an increase in the cobalt content, although this did not appear to influence the fact that the catalyst Co_{20}/γ-Al_2O_3-CeO_2 had higher catalytic activity. It is important to note that the greater reducibility of Co_{10}/γ-Al_2O_3-CeO_2 did not translate into higher VOC oxidation activity. However, other factors to be considered are the presence of active sites, such as Co^{2+} and Co^{3+} ions, strong interaction between the oxide phases and oxygen vacancies on the Co_{20}/γ-Al_2O_3-CeO_2 catalyst surface as confirmed by the characterization results discussed above, which is related to the oxidation of hydrocarbons (Cordatos *et al*., 1996; Lefez *et al*., 1996; Putna *et al*., 1999; Volta and Portefaix, 1985; Todorova *et al*., 2009; Todorova *et al*., 2011). The cobalt enrichment on the catalyst surface (as evidenced by the XPS data) may have contributed to the higher activity observed for the Co_{20}/γ-Al_2O_3-CeO_2 catalyst, since cobalt is a very active species in oxidation reactions. With an increase in the cobalt loading, a higher number of active sites are available

for the oxidation reactions, which resulted in higher conversion levels. As shown in Table 2, the lower Co/Ce ratio of the Co_{10}/γ-Al_2O_3-CeO_2 catalyst can be explained by the partial coating of the cobalt oxide by cerium oxide, which can block some of the active cobalt sites reflecting in a lower activity (Todorova *et al*., 2010). In addition, Kang *et al*. (2003), studying cobalt supported on ceria catalysts in the CO oxidation reaction, concluded that ceria supplies oxygen to cobalt, leading to the retention of its higher valence state with increasing cobalt loading. This effect of ceria contributing to maintaining the high valence state of CoO_x species improves the catalytic activity in oxidation reactions (Kang et al., 2003; Liotta *et al*., 2005). Another factor to be considered is the mobility of the oxygen atoms present, which are able to perform the oxidation of the hydrocarbons under study. It has been reported that the presence of oxygen vacancies is an important factor that influences the activity of some heterogeneous catalysts and favors the oxidation process (Luo *et al*., 2008; Tian *et al*., 2012; Todorova *et al*., 2012). An increase in the amount of oxygen vacancies can result in an enhancement of the bulk and surface oxygen mobility, which is believed to play an important role in oxidation reactions (Liotta *et al*., 2005; Soykal *et al*., 2012a; Sun *et al*., 2008). The higher oxygen mobility benefits the oxygen species migration across the catalyst structure, resulting in higher oxidation activity (Song *et al*., 2009). It has been shown that the reduction in cerium oxide (Ce^{+4}/Ce^{+3}) is not due to a direct release of oxygen into the gas phase, but rather to the interaction which occurs between the surface of the catalyst and the hydrocarbon (Putna *et al*., 1999; Suresh *et al*., 2012; Todorova *et al*., 2009; Todorova *et al*., 2012). These reactions are driven by the increased capacity for the spontaneous release of oxygen from the Co_3O_4/CeO_2 system, even in the absence of a reducing agent. In the presence of the Co_3O_4 species, the catalyst promotes the reduction of Ce^{+4}/Ce^{+3}, this factor being favorable for the oxidation of hydrocarbons (Warang *et al*., 2012). The addition of cobalt in the CeO_2 structure reduces the lattice parameter, suggesting the incorporation of Co_3O_4 by way of Co-O-Ce bonds (Kang *et al*., 2003; Murgida *et al*., 2012). It is well known that the oxidation of hydrocarbons promoted by solid oxide catalysts (including cerium oxide catalysts) can proceed via the Mars and van Krevelen mechanism in which the key steps are the supply of oxygen by the reducible oxide, the introduction of the oxygen species from the lattice oxide into the substrate molecule, and the re-oxidation of the reduced solid by the oxygen-containing gaseous phase, the rate-determining step of the reaction (Menezo *et al*., 1993; Todorova *et al*., 2012). According to Todorova *et al*. (2009**)**, the oxygen storage capacity of cerium oxide is associated with a fast Ce^{4+}/Ce^{3+} redox process, making more oxygen available for the oxidation process. The oxygen migration on the catalyst surface is important in oxidation reactions, where the oxidation-reduction cycles determine the catalytic activity. Thus, the redox properties of the catalyst play a key role in the process and are an important factor in determining the catalytic performance. The Co_{20}/γ-Al_2O_3-CeO_2 catalyst possesses a higher amount of oxygen vacancies and additionally it is probable that the large crystal size, good stability, close contact between cobalt and the support particles and higher cobalt surface concentration would favor the catalytic performance of the Co_{20}/γ-Al_2O_3-CeO_2 catalytic system. These characteristics were verified by the XRD, N_2-physisorption, O_2-chemisorption, TPR, XPS and TEM results. It is interesting to note that in our experiments the γ-Al_2O_3, CeO_2 and γ-Al_2O_3-CeO_2 supports showed no appreciable catalytic activity in the oxidation of VOCs, as shown in Fig. 8, indicating the effective action of cobalt species and the synergetic effect of the interaction between the cobalt and the aluminum and cerium oxides, which improves the catalytic activity of the cobalt-based catalytic system in the oxidation reactions (Silva *et al*., 2004; Abbasi *et al.,* 2011; Solsona *et al*., 2012; Gómez *et al*., 2012).

Catalytic oxidation can be influenced by the structure of the organic compound. Thus, under the same reaction conditions different levels of activity are expected for different VOCs. It can be observed from Fig. 8 that over the Co_{20}/γ-Al_2O_3-CeO_2 catalyst the almost complete conversion (around 96%) of n-hexane was achieved at 350 °C, while the conversions for benzene, toluene and o-xylene at this reaction temperature were approximately 89, 70 and 57%, respectively. Interestingly, it can be observed that n-hexane is oxidized more readily than the aromatic compounds, even though the combustion of alkanes generally does not occur as easily as that of aromatic compounds. In the latter case, when these compounds are associated with methyl groups they are not as easily oxidized as benzene (Wu *et al.,* 2000; Abbasi *et al.,* 2011).

CONCLUSIONS

The Co_{10}/γ-Al_2O_3-CeO_2 and Co_{20}/γ-Al_2O_3-CeO_2 catalysts showed good activity in the oxidation of volatile organic compounds (n-hexane, benzene,

toluene and o-xylene). The conversion level was found to be dependent on the VOC to be oxidized. The enrichment of cobalt on the catalyst surface contributes to higher catalytic activity as observed for the catalyst Co_{20}/γ-Al_2O_3-CeO_2. With an increased cobalt load, a greater number of active sites become available for oxidation reactions, resulting in higher levels of conversion. The presence of ceria in the catalysts can supply oxygen to cobalt, which retains its higher valence state, with an increase in the cobalt loading contributing to higher catalytic activity. The superior performance of the Co_{20}/γ-Al_2O_3-CeO_2 catalyst may also be attributed to its higher amount of oxygen vacancies and stronger contact between the cobalt, cerium and aluminum oxides.

ACKNOWLEDGMENTS

The authors acknowledge the financial support provided by CNPq, FAPEMIG, LCME-UFSC and INCT.

REFERENCES

Andreeva, D., Tabakova, T., Ilieva, L., Naydenov, A., Mehanjiev, D., Abrashev, M. V., Nanosize gold catalysts promoted by vanadium oxide supported on titania and zirconia for complete benzene oxidation. Appl. Catal. A-Gen., 209, 291-300 (2001).

Abbasi, Z., Haghighi, M., Fatehifar, E., Saedy, S., Synthesis and physicochemical characterizations of nanostructured Pt/Al_2O_3-CeO_2 catalysts for total oxidation of VOCs. J. Hazard. Mater., 186, 1445-1454 (2011).

Barakat, T., Rooke, J. C., Franco, M., Cousin, R., Lamonier, J-F., Giraudon, J-M., Su, B-L., Siffert, S., Pd- and/or Au-loaded Nb- and V-doped macro-mesoporous TiO_2 supports as catalysts for the total oxidation of VOCs. Eur. J. Inorg. Chem., 16, 2812-2818 (2012).

Barreiro, E., Gea, J., Sanjuas, C., Marcos, R., Broquetas, J., Milic-Emili, J., Dyspnoea at rest and at the end of different exercises in patients with near-fatal asthma. Eur. Respir. J., 24, 219-225 (2004).

Beche, E., Charvin, P., Perarnau, D., Abanades, S., Flamant, G., Ce 3d XPS investigation of cerium oxides and mixed cerium oxide (CexTiyOz). Surf. Int. Anal., 40, 264-267 (2008).

Beche, E., Peraudeau, G., Flaud, V., Perarnau, D., An XPS investigation of (La2O3)1-x (CeO2)2x (ZrO2)2 compounds. Surf. Int. Anal., 44, 1045-1050 (2012).

Calvo, J. H., Marcos, S., Jurado, J. J., Serrano, M., Association of the heart fatty acid-binding protein (FABP3) gene with milk traits in Manchega breed sheep. Anim. Genet., 35, 347-349 (2004).

Cordatos, H., Ford, D., Gorte, R. J., Simulated annealing study of the structure and reducibility in ceria clusters. J. Phys. Chem-Us., 100, 18128-18132 (1996).

Corma, A., From microporous to mesoporous molecular sieve materials and their use in catalysis. Chem. Ver., 97, 2373-2419 (1997).

Garcia, S. R., Assaf, J. M., Effect of the preparation method on Co/Al_2O_3 catalyst applied to ethanol steam reforming reaction production of hydrogen. Modern Research in Catalysis, 1, 52-57 (2012).

Garcia-Vazquez, E., Marcos, M. A., Mensa, J., de Roux, A., Puig, J., Font, C., Francisco, G., Torres, A., Assessment of the usefulness of sputum culture for diagnosis of community-acquired pneumonia using the PORT predictive scoring system. Arch. Intern. Med., 164, 1807-1811 (2004).

Genuino, H. C., Dharmarathna, S., Njagi, E. C., Mei, M. C., Suib, S. L., Gas-phase total oxidation of benzene, toluene, ethylbenzene, and xylenes using shape-selective manganese oxide and copper manganese oxide catalysts. J. Phys. Chem. C., 116, 12066-12078 (2012).

Gomez, L. E., Tiscornia, I. S., Boix, A. V., Miro, E. E., CO preferential oxidation on cordierite monoliths coated with Co/CeO_2 catalys. Int. J. Hydrogen. Energ., 37, 14812-14819 (2012).

Holgado, J. P., Alvarez, R., Munuera, G., Study of CeO_2 XPS spectra by factor analysis: reduction of CeO_2. Appl. Surf. Sci., 161, 301-315 (2000).

Hu, X., Lu, G., Acetic acid steam reforming to hydrogen over $Co\text{-}Ce/Al_2O_3$ and $Co\text{-}La/Al_2O_3$ catalysts – The promotion effect of Ce and La addition. Catal. Commun., 12, 50-53 (2010).

Kang, M., Song, M. W., Lee, C. H., Catalytic carbon monoxide oxidation over CoO_x/CeO_2 composite catalysts. Appl. Catal. A-Gen., 251, 143-156 (2003).

Kim, S. C., The catalytic oxidation of aromatic hydrocarbons over supported metal oxide. J. Hazard. Mater., B91, 285-299 (2002).

Kim, S. C., Shim, W. G., Catalytic combustion of VOCs over a series of manganese oxide catalysts. Appl. Catal. B-Environ., 98, 180-185 (2010).

Kirchnerova, J., Alifanti, M., Delmon, B., Evidence of phase cooperation in the $LaCoO_3$-CeO_2-Co_3O_4 catalytic system in relation to activity in methane combustion. Appl. Catal. A-Gen., 231, 65-80 (2002).

Kirchnerova, J., Klvana, D., Design criteria for high-temperature combustion catalysts. Catal. Lett., 67, 175-181 (2000).

Lakshmi, Y. K., Srinivas, K., Sreedhar, B., Raja, M. M., Vithal, M., Reddy, P. V., Structural, optical and magnetic properties of nanocrystalline Zn0.9Co0.1O-based diluted magnetic semiconductors. Mater. Chem. Phys., 113, 749-755 (2009).

Lefez, B., Nkeng, P., Lopitaux, J., Poillerat, G., Characterization of cobaltite spinels by reflectance spectroscopy. Mater. Res. Bull., 31, 1263-1267 (1996).

Liotta, L. F., Catalytic oxidation of volatile organic compounds on supported noble metals. Appl. Catal. B-Environ., 100, 403-412 (2010).

Liotta, L. F., Di Carlo, G., Pantaleo, G., Deganello, G., Co_3O_4/CeO_2 and Co(3)O(4)/CeO_2-ZrO_2 composite catalysts for methane combustion: Correlation between morphology reduction properties and catalytic activity. Catal. Commun., 6, 329-336 (2005).

Lovon, A. S. P., Lovon-Quintana, J. J., Almerindo, G. I., Valenca, G. P., Bernardi, M. I. B., Araujo, V. D., Rodrigues, T. S., Robles-Dutenhefner, P. A., Fajardo, H. V., Preparation, structural characterization and catalytic properties of Co/CeO_2 catalysts for the steam reforming of ethanol and hydrogen production. J. Power Sources., 216, 281-289 (2012).

Luo, J. Y., Meng, M., Li, X., Li, X. G., Zha, Y. Q., Hu, T. D., Xie, Y. N., Zhang, J., Mesoporous Co(3)O(4)-CeO(2) and Pd/Co(3)O(4)-CeO(2) catalysts: Synthesis, characterization and mechanistic study of their catalytic properties for low-temperature CO oxidation. J. Catal., 254, 310-324 (2008).

Mamontov, E., Egami, T., Brezny, R., Koranne, M., Tyagi, S., Lattice defects and oxygen storage capacity of nanocrystalline ceria and ceria-zirconia. J. Phys. Chem., B, 104, 11110-11116 (2000).

Marcos, J., de la Torre, X., Gonzalez, J. C., Segura, J., Pascual, J. A., Liquid chromatography clean-up method to improve identification of anabolic agents in human urine by gas chromatography-mass spectrometry. Anal. Chim. Acta, 522, 79-88 (2004).

Menezo, J. C., Riviere, J., Barbier, J., Effect of the doping of a metal-oxide by platinum on its oxidizing properties. React. Kinet. Catal. Lett., 49, 293-298 (1993).

Murgida, G. E., Vildosola, V., Ferrari, V., Llois, A. M., Charge localization in Co-doped ceria with oxygen vacancies. Solid. State. Commun., 152, 368-371 (2012).

Putna, E. S., Bunluesin, T., Fan, X. L., Gorte, R. J., Vohs, J. M., Lakis, R. E., Egami, T., Ceria films on zirconia substrates: Models for understanding oxygen-storage properties. Catal. Today, 50, 343-352 (1999).

Salim, M. A., Khawaja, E. E., X-ray photoelectron-spectroscopy study of sodium germanate glass containing cobalt oxide. J. Non-Cryst. Solids., 151, 71-80 (1992).

Setiabudi, A., Chen, J. L., Mul, G., Makkee, M., Moulijn, J. A., CeO_2 catalysed soot oxidation - The role of active oxygen to accelerate the oxidation conversion. Appl. Catal. B-Environ., 51, 9-19 (2004).

Silva, A. M. T., Marques, R. R. N., Quinta-Ferreira, R. M., Catalysts based in cerium oxide for wet oxidation of acrylic acid in the prevention of environmental risks. Appl. Catal. B-Environ., 47, 269-279 (2004).

Song, H., Ozkan, U. S., Ethanol steam reforming over Co-based catalysts: Role of oxygen mobility. J. Catal., 261, 66-74 (2009).

Soykal, I. I., Bayram, B., Sohn, H., Gawade, P., Miller, J. T., Ozkan, U. S., Ethanol steam reforming over Co/CeO_2 catalysts: Investigation of the effect of ceria morphology. Appl. Catal. a-Gen., 449, 47-58 (2012).

Soykal, I. I., Sohn, H., Ozkan, U. S., Effect of support particle size in steam reforming of ethanol over Co/CeO_2 catalysts. ACS. Catal., 2, 2335-2348 (2012).

Spadaro, L., Arena, F., Granados, M. L., Ojeda, M., Fierro, J. L. G., Frusteri, F., Metal–support interactions and reactivity of Co/CeO_2 catalysts in the Fischer-Tropsch synthesis reaction. J. Catal., 234, 451-462 (2005).

Sun, G. B., Hidajat, K., Wu, X. S., Kawi, S., A crucial role of surface oxygen mobility on nanocrystalline Y_2O_3 support for oxidative steam reforming of ethanol to hydrogen over Ni/Y_2O_3 catalysts. Appl. Catal. B-Environ., 81, 303-312 (2008).

Suresh, G., Saravanan, P., Babu, D. R., Effect of annealing on phase composition, structural and magnetic properties of Sm-Co based nanomagnetic material synthesized by sol-gel process. J. Magn. Magn. Mater., 324, 2158-2162 (2012).

Solsona, B., Pérez-Cabero, M., Vázquez, I., Dejoz, A., García, T., Álvarez-Rodríguez, J., El-Haskouri, J., Beltrán, D., Amorós, P., Total oxidation of VOCs on Au nanoparticles anchored on Co doped mesoporous UVM-7 silica. Chem. Eng. J., 187, 391-400 (2012).

Tian, Z. Y., Ngamou, P. H. T., Vannier, V., Kohse-Hoinghaus, K., Bahlawane, N., Catalytic oxidation

of VOCs over mixed Co-Mn oxides. Appl.Catal. B-Environ., 117, 125-134 (2012).

Todorova, S., Kadinov, G., Tenchev, K., Caballero, A., Holgado, J. P., Pereniguez, R., Co_3O_4 + CeO_2/SiO_2 Catalysts for n-Hexane and CO Oxidation. Catal. Lett., 129, 149-155 (2009).

Todorova, S., Kolev, H., Holgado, J. P., Kadinov, G., Bonev, Ch., Pereñíguez, R., Caballero, A., Complete n-hexane oxidation over supported Mn-Co catalysts. Appl. Catal. B-Environ., 94, 46-54 (2010).

Todorova, S., Naydenov, A., Kolev, H., Holgado, J. P., Ivanov, G., Kadinov, G., Caballero, A., Mechanism of complete n-hexane oxidation on silica supported cobalt and manganese catalysts. Appl. Catal. A-Gen., 413, 43-51 (2012).

Todorova, S., Naydenov, A., Kolev, H., Tenchev, K., Ivanov, G., Kadinov, G., Effect of Co and Ce on silica supported manganese catalysts in the reactions of complete oxidation of n-hexane and ethyl acetate. J. Mater. Sci., 46, 7152-7159 (2011).

Volta, J. C., Portefaix, J. L., Structure sensitivity of mild oxidation reactions on oxide catalysts - a review. Appl. Catal., 18, 1-32 (1985).

Wang, H., Ye, J. L., Liu, Y., Li, Y. D., Qin, Y. N., Steam reforming of ethanol over Co_3O_4/CeO_2 catalysts prepared by different methods. Catal. Today., 129, 305-312 (2007).

Warang, T., Patel, N., Santini, A., Bazzanella, N., Kale, A., Miotello, A., Pulsed laser deposition of Co_3O_4 nanoparticles assembled coating: Role of substrate temperature to tailor disordered to crystalline phase and related photocatalytic activity in degradation of methylene blue. Appl. Catal. A-Gen., 423, 21-27 (2012).

Wu, J. C. S., Lin, Z. A., Tsai, F. M., Pan, J. W., Low-temperature complete oxidation of BTX on Pt/ activated carbon catalysts. Catal. Today, 63 419-426 (2000).

Wu, H., Wang, L., Shen, Z., Zhao, J., Catalytic oxidation of toluene and p-xylene using gold supported on Co_3O_4 catalyst prepared by colloidal precipitation method. J. Mol. Catal. A-Chem., 351, 188-195 (2011).

Zhang, C., Li, S., Li, M., Wang, S., Ma, X., Gong, J., Enhanced oxygen mobility and reactivity for ethanol steam reforming. AIChE J., 58, 516-525 (2012).